J. Fluid Mech. (1982), *vol.* 117, *pp.* 143-170
Printed in Great Britain

General theory for the creeping motion of a finite sphere along the axis of a circular orifice

By Z. DAGAN,

Institute of Applied Chemical Physics, The City College of The City University of New York, New York

S. WEINBAUM

Department of Mechanical Engineering, The City College of The City University of New York, New York

AND R. PFEFFER

Department of Chemical Engineering, The City College of The City University of New York, New York

(Received 30 January 1981 and in revised form 10 August 1981)

This paper presents the first infinite-series solutions to the creeping-flow equations for the axisymmetric motion of a sphere of arbitrary size towards an orifice whose diameter is either larger or smaller than the sphere. To obtain the solution the flow field is partitioned in the plane of the opening, and for the flow to the left and right of the fluid interface separate solutions are developed that satisfy the viscous-flow boundary conditions in each region and unknown functions for the axial and radial velocity components in the plane of the opening. The continuity of the fluid stress tensor at the matching interface leads to a set of dual integral equations which are solved analytically to determine the unknown functions for the velocity components in the matching plane. A boundary collocation technique is used to satisfy the no-slip boundary conditions on the surface of the sphere.

The accuracy and convergence of the present solution is tested by detailed numerical comparison with the exact bipolar co-ordinate solutions of Brenner (1961) for the drag on a sphere translating perpendicular to an infinite plane wall up to a distance of 0·1 sphere radii and is found to be in agreement to five significant digits. The converged-series collocation solutions are presented for the sphere in motion in quiescent fluid or for flow past a rigidly held sphere positioned axisymmetrically near a fixed orifice. Solutions are also presented for the zero-drag velocity of a neutrally buoyant sphere in a flow through an orifice, and the pressure–volume flow relation for a ball-valve geometry.

1. Introduction

It is well recognized that the creeping motion of a spherical particle at finite distances from a boundary or orifice can require a very substantial correction to Stokes' law for the resistance of a sphere moving in an unbounded fluid. These corrections are particularly important when the sphere–wall spacing is of the order of five sphere diameters or less, where the weak-interaction method of reflection theory

breaks down (see Ganatos, Weinbaum & Pfeffer 1980). All previous exact solutions for bounded flows of a sphere have involved infinite planar or cylindrical surfaces (Haberman & Sayre 1958; Brenner 1961; Goldman, Cox & Brenner, 1967*a*, *b*). More recently, Davis, O'Neill & Brenner (1981) obtained first-order expressions for the effect of an orifice in a plane wall upon the hydrodynamic force and torque acting on a stokeslet or rotlet situated along the axis of the orifice. In this paper we shall consider the on-axis motion of a finite sphere that is either smaller or larger than the orifice opening. Highly accurate series-truncation solutions are presented for the motion of a sphere in quiescent fluid, the flow past a fixed sphere, the motion of a neutrally buoyant sphere, and the pressure–volume flow relationship for the flow through the orifice that are valid up to the point where the sphere is tangent to the plane of the orifice. A companion paper for the complementary geometry, a sphere situated coaxially in the stagnation region near a finite disk, is currently under review. Both problems are of intrinsic mathematical interest because of their role in the theory of mixed-boundary-value problems. The problem is further complicated by the absence of a natural co-ordinate system that can be used to satisfy the no-slip boundary conditions simultaneously on the discontinuous planar boundary and on the sphere. The creeping motion of a sphere near an infinite planar boundary, on the other hand, can be treated as a special case of the spherical bipolar co-ordinate system in which the infinite plane is taken as a sphere of infinitely large radius. The use of this co-ordinate system allowed Brenner (1961) and Goldman *et al.* (1967*a*, *b*) to obtain exact solutions for the motion of a sphere perpendicular and parallel to an infinite plane wall.

The motion of a sphere approaching an orifice is of interest in a variety of biological and non-biological phenomena. Some biological applications include molecular-sieving effects at the entrance to pores in biological membranes, the filling of open attached plasmalemma vesicles with plasma proteins and the entrance effects that result when micron-sized particles, such as red cells, enter a narrow tube from a feed reservoir (Fahraeus & Lindqvist 1931). An important non-biological application is the nuclepore filter. All existing theoretical solution studies of the nuclepore filter have neglected the boundary conditions on the surface of the particle and hence have omitted the effect of the particle on the local flow at the pore entrance. Another application is the operation of a ball valve at low Reynolds number.

To treat theoretically the motion of a sphere towards an orifice we have divided the flow field into two simply bounded regions: the half-space containing the sphere and bounded by the orifice wall, and the remaining infinite half-space. This partitioning of the flow field establishes well-defined regions in which the solution for the velocity distribution can be obtained in terms of the unknown velocity profile at the orifice opening. Different stream-function representations are chosen for each region and are matched analytically at the orifice opening to secure continuity of the kinematic and dynamic fields. The no-slip boundary conditions on the surface of the sphere can be satisfied by making use of the collocation technique described in detail in Ganatos, Pfeffer & Weinbaum (1978). A successful application of the collocation technique depends primarily on the feasibility of representing by a suitable integral transform the disturbances generated by the sphere and felt on the confining boundary. The inversion of this integral transform, which can be mathematically difficult, has to be performed analytically in order to reduce computation time to acceptable limits.

The combined analytical–numerical solution procedure used in this problem is an important extension of the collocation theory first developed by Gluckman, Pfeffer & Weinbaum (1971) for unbounded axisymmetric multisphere Stokes flow. The technique has also been applied to axisymmetric flows with infinite cylindrical boundaries by Leichtberg, Pfeffer & Weinbaum (1976) for the coaxial creeping motion of finite clusters of spheres in a tube and recently extended to fully three-dimensional bounded motions by Ganatos, Weinbaum & Pfeffer (1980; also Ganatos, Pfeffer & Weinbaum 1980) for the arbitrary motion of a sphere between plane-parallel boundaries. The method of solution used in the present study is the first to incorporate the collocation method in a partitioned flow field with discontinuous planar boundaries.

In view of the linearity of the governing differential equations and the boundary conditions, the axisymmetric motion of a neutrally buoyant sphere towards an orifice can be decomposed into two separate contributions: (i) a translational motion of a sphere in quiescent fluid, and (ii) flow through an orifice past a stationary sphere. The paper is presented in six sections. Section 2 contains the mathematical formulation of the problem. In §3, solutions for the motion of a sphere in a quiescent fluid are presented. The case of flow through an orifice past a stationary sphere is described in §4. In §5, results for the pressure drop across the orifice are presented. In §6 the two cases are superposed to determine the motion of a neutrally buoyant sphere towards the orifice.

2. Mathematical formulation

The flow field under consideration consists of a solid sphere of radius a' moving axially with an instantaneous velocity V' in viscous fluid towards an orifice of radius b' in a wall of zero thickness whose distance from the sphere is d'. The origin of co-ordinates is chosen at the sphere centre. The proposed theory is valid up to the point where the sphere is tangent to the plane of the orifice. Before presenting the equations of motion it is convenient to non-dimensionalize the co-ordinates (unprimed) in terms of the dimensional (primed) co-ordinates (figure 1), as follows:

$$R = \frac{R'}{b'}, \quad z = \frac{z'}{b'}, \tag{2.1a, b}$$

such that the dimensionless sphere radius and its distance from the orifice are respectively

$$a = \frac{a'}{b'}, \quad d = \frac{d'}{b'}. \tag{2.2a, b}$$

The stream function ψ', the drag force F', and the pressure P', are expressed in dimensionless form using the fluid density ρ, the kinematic viscosity ν and the characteristic length b' as follows:

$$\psi = \frac{\psi'}{b'\nu}, \quad F = \frac{F'}{\rho\nu^2}, \quad P = \frac{P'b'^2}{\rho\nu^2}. \tag{2.3a, b, c}$$

The governing equations for the fluid motion are

$$\nabla^2\mathbf{u} = \nabla P, \quad \nabla.\mathbf{u} = 0, \tag{2.4a, b}$$

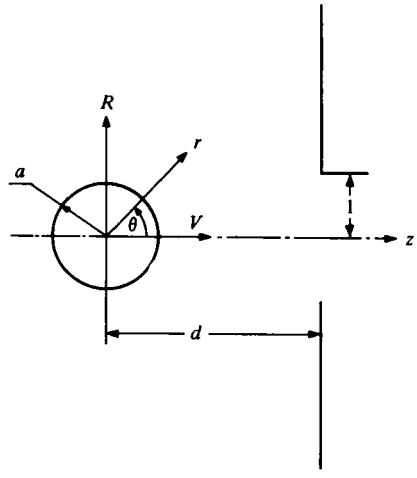

FIGURE 1. Geometry for the problem of a sphere translating axisymmetrically towards an orifice.

where ∇ is the gradient operator in dimensionless co-ordinates. Owing to the axisymmetric nature of the flow, the stream function can be introduced, and is given in cylindrical co-ordinates:

$$u_R = -\frac{1}{R}\frac{\partial \psi}{\partial z}, \quad u_z = \frac{1}{R}\frac{\partial \psi}{\partial R}, \tag{2.5a, b}$$

where u_R and u_z are the radial and axial velocity components respectively. Taking the curl of (2.4) and using the definition of the stream function (2.5) yields the fourth-order equation

$$D^2(D^2\psi) = 0, \tag{2.6}$$

where D^2 is the generalized axisymmetric Stokesian operator given by

$$D^2 = \frac{\partial^2}{\partial R^2} - \frac{1}{R}\frac{\partial}{\partial R} + \frac{\partial^2}{\partial z^2}. \tag{2.7}$$

As discussed in §1, we partition the flow field into two regions, the half-space containing the sphere, $z \leqslant d$, and the infinite half-space, $z \geqslant d$. The essential mathematical problem is to match kinematically and dynamically the solution in each region at the orifice opening.

The stream function for the region $z \leqslant d$ is linearly composed of two parts:

$$\psi^{\mathrm{I}} = \psi_{\mathrm{w}} + \psi_{\mathrm{s}}. \tag{2.8}$$

Here ψ_{w} is a solution of (2.6) in cylindrical co-ordinates that represents the disturbances generated by the orifice and the wall approaching the plane $z = d$ from the left and which yields finite velocities everywhere for $z \leqslant d$. ψ_{w} is given by a Fourier–Bessel integral:

$$\psi_{\mathrm{w}} = \int_0^\infty RJ_1(\omega R)\,[A_1(\omega) + zB_1(\omega)]\,e^{\omega z}\,d\omega \quad (z \leqslant d), \tag{2.9}$$

where $A_1(\omega)$ and $B_1(\omega)$ are unknown functions of ω, and J_1 is the ordinary Bessel function of the first kind of order 1.

The second part of ψ^{I}, denoted by ψ_s, is an infinite series representing the disturbance generated by the sphere. ψ_s is given by all the simply separable solutions of (2.6) in spherical co-ordinates that yield a finite velocity everywhere. This series is given by Sampson (1891) as

$$\psi_s = \sum_{n=2}^{\infty} (B_n r^{-n+1} + D_n r^{-n+3}) I_n(\xi) \quad (z \leqslant d). \tag{2.10}$$

Here r and θ are the spherical co-ordinates shown in figure 1, $\xi = \cos\theta$, and I_n is the Gegenbauer function of the first kind of order n and degree $-\frac{1}{2}$. B_n and D_n are unknown constant coefficients to be determined by satisfying the no-slip boundary conditions on the sphere.

For the infinite half-space $z \geqslant d$, it is sufficient to represent all disturbances generated at the plane $z = d$ by a Fourier–Bessel integral of the form given by (2.9), which yields finite velocity as z approaches infinity:

$$\psi^{\mathrm{II}} = \int_0^{\infty} RJ_1(\omega R)\,[A_2(\omega) + zB_2(\omega)]\,e^{-\omega z}\,d\omega \quad (z \geqslant d). \tag{2.11}$$

Here $A_2(\omega)$ and $B_2(\omega)$ are unknown functions of ω.

To help the reader follow the mathematical development, we give below a brief conceptual summary of the solution procedure to determine the unknown coefficients.

In each region the no-slip boundary conditions are first satisfied along the orifice wall. This permits the unknown functions $A_1(\omega)$ and $B_1(\omega)$ to be determined in terms of the spherical coefficients B_n and D_n and the unknown velocity at the orifice opening. Similarly, $A_2(\omega)$ and $B_2(\omega)$ can be determined in terms of the unknown velocity at the orifice plane. Then, by matching the stress tensor at the opening of the orifice, the unknown orifice velocity can be obtained in terms of the spherical coefficients. This matching assures that the disturbances produced by the sphere for all values of B_n and D_n are cancelled along the boundary of $z = d$ approaching the orifice wall from both the left and right. Finally, the cancellation of the disturbances generated on the surface of the sphere by the orifice wall will be accomplished by applying the collocation method. The solution of the collocation matrix provides numerical values for the coefficients B_n and D_n.

In order to apply the no-slip boundary conditions along the wall of the plane of the orifice it is necessary to write the spherical-disturbance equation (2.8) in cylindrical co-ordinates. Therefore, the spherical co-ordinate system (r, θ) has to be related to the cylindrical co-ordinate system (R, z). From figure 1, the co-ordinate transformation is given by

$$r = (R^2 + z^2)^{\frac{1}{2}}, \quad \theta = \arccos\,[z(R^2 + z^2)^{-\frac{1}{2}}]. \tag{2.12}$$

Differentiation of (2.8) according to (2.5) utilizing the properties of the Gegenbauer and Legendre polynomials and the chain rule, yields the expressions for the radial and axial velocity components for the half-space $z \leqslant d$:

$$u_R^{\mathrm{I}} = -\frac{1}{R}\frac{\partial \psi^{\mathrm{I}}}{\partial z} = -\int_0^{\infty} k_1'(\omega, z)\,\omega J_1(\omega R)\,d\omega + \sum_{n=2}^{\infty} [B_n B_n'(R, z) + D_n D_n'(R, z)], \tag{2.13a}$$

$$u_z^{\mathrm{I}} = \frac{1}{R}\frac{\partial \psi^{\mathrm{I}}}{\partial R} = \int_0^{\infty} k_2''(\omega, z)\,\omega J_0(\omega R)\,d\omega + \sum_{n=2}^{\infty} [B_n B_n''(R, z) + D_n D_n''(R, z)], \tag{2.13b}$$

where

$$k_1'(\omega, z) = \left[A_1(\omega) + B_1(\omega)\left(\frac{1}{\omega} + z\right)\right] e^{\omega z}, \tag{2.14a}$$

$$B_n'(R, z) = \frac{n+1}{(R^2+z^2)^{\frac{1}{2}n}} \frac{1}{R} I_n\left(\frac{z}{(R^2+z^2)^{\frac{1}{2}}}\right), \tag{2.14b}$$

$$D_n'(R, z) = \frac{n+1}{(R^2+z^2)^{\frac{1}{2}(n-2)}} \frac{1}{R} I_{n+1}\left(\frac{z}{(R^2+z^2)^{\frac{1}{2}}}\right) - \frac{2}{(R^2+z^2)^{\frac{1}{2}(n-1)}} \frac{z}{R} I_n\left(\frac{z}{(R^2+z^2)^{\frac{1}{2}}}\right), \tag{2.14c}$$

$$k_1''(\omega, z) = [A_1(\omega) + zB_1(\omega)] e^{\omega z}, \tag{2.14d}$$

$$B_n''(R, z) = \frac{1}{(R^2+z^2)^{\frac{1}{2}(n+1)}} P_n\left(\frac{z}{(R^2+z^2)^{\frac{1}{2}}}\right), \tag{2.14e}$$

$$D_n''(R, z) = \frac{2}{(R^2+z^2)^{\frac{1}{2}(n-1)}} I_n\left(\frac{z}{(R^2+z^2)^{\frac{1}{2}}}\right) + \frac{1}{(R^2+z^2)^{\frac{1}{2}(n-1)}} P_n\left(\frac{z}{(R^2+z^2)^{\frac{1}{2}}}\right), \tag{2.14f}$$

and P_n are Legendre polynomials of order n. Similarly, for the region $z \geqslant d$, the velocity components are obtained by differentiation of (2.11), and are given by

$$u_R^{\mathrm{II}} = -\frac{1}{R}\frac{\partial \psi^{\mathrm{II}}}{\partial z} = -\int_0^\infty k_2'(\omega, z)\, \omega J_1(\omega R)\, d\omega, \tag{2.15a}$$

$$u_z^{\mathrm{II}} = \frac{1}{R}\frac{\partial \psi^{\mathrm{II}}}{\partial R} = \int_0^\infty k_2''(\omega, z)\, \omega J_0(\omega R)\, d\omega, \tag{2.15b}$$

where

$$k_2'(\omega, z) = -\left[A_2(\omega) - B_2(\omega)\left(\frac{1}{\omega} - z\right)\right] e^{-\omega z}, \tag{2.16a}$$

$$k_2''(\omega, z) = [A_2(\omega) + zB_2(\omega)] e^{-\omega z}. \tag{2.16b}$$

The no-slip boundary conditions along the wall of the orifice can now be applied, provided that the velocity at the orifice is prescribed. This velocity can be defined as follows:

$$\mathbf{u}(R, d) = \frac{1}{R}[f(R)\hat{\mathbf{z}} - g(R)\hat{\mathbf{r}}] \quad (0 \leqslant R \leqslant 1), \tag{2.17}$$

where $f(R)/R$ and $-g(R)/R$ are the unknown axial and radial velocity components at the opening respectively. From the definition (2.17) the no-slip boundary conditions on the orifice wall are (i = I, II)

$$u_z^i(R, d) = F(R) = \begin{cases} 0 & (R > 1), \\ f(R)/R & (0 \leqslant R \leqslant 1,) \end{cases} \tag{2.18a}$$

$$u_R^i(R, d) = G(R) = \begin{cases} 0 & (R > 1), \\ -g(R)/R & (0 \leqslant R \leqslant 1). \end{cases} \tag{2.18b}$$

In addition, the stress tensor has to be matched along the interface between the two regions; this dynamic boundary condition is

$$\tau_{ij}^{\mathrm{I}}(R, d) = \tau_{ij}^{\mathrm{II}}(R, d) \quad (0 \leqslant R \leqslant 1), \tag{2.19}$$

where τ_{ij} is the stress tensor.

Following the solution summary given previously, we now need to determine the Fourier coefficients $A_i(\omega)$, $B_i(\omega)$, $i = 1, 2$.

Application of the kinematic boundary conditions (2.18) along the wall in the half-space containing the sphere results in

$$\int_0^\infty k_1'(\omega,d)\,\omega J_1(\omega R)\,d\omega = \sum_{n=2}^{\infty}[B_n B_n'(R,d)+D_n D_n'(R,d)]-G(R), \tag{2.20a}$$

$$\int_0^\infty k_1''(\omega,d)\,\omega J_0(\omega R)\,d\omega = -\sum_{n=2}^{\infty}[B_n B_n''(R,d)+D_n D_n''(R,d)]+F(R). \tag{2.20b}$$

The right-hand side in (2.20) represents the disturbance generated by the sphere and the orifice opening which must be cancelled on the orifice wall. The unknown functions k_1' and k_1'' in (2.20) evaluated at $z = d$, are simply Hankel transforms of these disturbances. Inversion of these equations gives

$$k_1'(\omega,d) = \int_0^\infty \sum_{n=2}^{\infty}[B_n B_n'(t,d)+D_n D_n'(t,d)]\,tJ_1(\omega t)\,dt+\int_0^1 g(t)\,J_1(\omega t)\,dt, \tag{2.21a}$$

$$k_1''(\omega,d) = -\int_0^\infty \sum_{n=2}^{\infty}[B_n B_n''(t,d)+D_n D_n''(t,d)]\,tJ_0(\omega t)\,dt+\int_0^1 f(t)\,J_0(\omega t)\,dt. \tag{2.21b}$$

The evaluation of the integrals in (2.21) and the determination of the functions $k_1'(\omega,z)$ and $k_1''(\omega,z)$ are shown in the appendix (equations (A 1)–(A 8)). Substituting these results into (2.13) and integrating the series provides the expressions for the radial and axial velocity components valid for $z \leqslant d$ in the form

$$u_R^{\mathrm{I}} = \int_0^\infty \left\{[\omega(d-z)-1]\int_0^1 g(t)\,J_1(\omega t)\,dt-\omega(d-z)\int_0^1 f(t)\,J_0(\omega t)\,dt\right\}\omega J_1(\omega R)\,e^{-\omega(d-z)}\,d\omega$$
$$+\sum_{n=2}^{\infty}[B_n\beta_n'(R,z)+D_n\delta_n'(R,z)], \tag{2.22a}$$

$$u_z^{\mathrm{I}} = \int_0^\infty \left\{[1+\omega(d-z)]\int_0^1 f(t)\,J_0(\omega t)\,dt-\omega(d-z)\int_0^1 g(t)\,J_1(\omega t)\,dt\right\}\omega J_0(\omega R)\,e^{-\omega(d-z)}\,d\omega$$
$$+\sum_{n=2}^{\infty}[B_n\beta_n''(R,z)+D_n\delta_n''(R,z)], \tag{2.22b}$$

where

$$\beta_n'(R,z) = B_n'(R,z)-B_n'(R,2d-z)+2(d-z)\,(n+1)\,B_{n+1}'(R,2d-z), \tag{2.23a}$$

$$\delta_n'(R,z) = D_n'(R,z)-D_n'(R,2d-z)-\frac{2}{n}(n-1)\,(n-3)\,(d-z)\,B_{n-1}'(R,2d-z)$$
$$+2(2n-3)\,d(d-z)\,B_n'(R,2d-z), \tag{2.23b}$$

$$\beta_n''(R,z) = B_n''(R,z)-B_n''(R,2d-z)-2(d-z)\,(n+1)\,B_{n+1}''(R,2d-z), \tag{2.23c}$$

$$\delta_n''(R,z) = D_n''(R,z)-D_n''(R,2d-z)+2(n-2)\,(d-z)\,B_{n-1}''(R,2d-z)$$
$$-2(2n-3)\,d(d-z)\,B_n''(R,2d-z). \tag{2.23d}$$

Although the velocities in (2.22) are still expressed in terms of the unknown spherical coefficients B_n and D_n, and the two unknown functions f and g, they do vanish on the walls of the orifice and can properly represent any arbitrary velocity profile at the opening.

Following a similar procedure, the no-slip boundary condition (2.18) can be satisfied in the infinite half-space $z \geqslant d$ and the Fourier coefficients $A_2(\omega)$ and $B_2(\omega)$ expressed in terms of the unknown functions f and g for the velocity at the orifice plane. These expressions are given in (A 9), (A 10) in the appendix. Substituting these results in equations (2.16a, b) one obtains

$$k_2'(\omega, z) = \left\{ -\omega(z-d) \int_0^1 f(t) J_0(\omega t)\, dt + [1-\omega(z-d)] \int_0^1 g(t) J_1(\omega t)\, dt \right\} e^{-\omega(z-d)}, \tag{2.24a}$$

$$k_2''(\omega, z) = \left\{ [1+\omega(z-d)] \int_0^1 f(t) J_0(\omega t)\, dt + \omega(z-d) \int_0^1 g(t) J_1(\omega t)\, dt \right\} e^{-\omega(z-d)}. \tag{2.24b}$$

Equations (2.24a, b) together with (2.15), provide the solution for the velocity field in the region $z \geqslant d$, in terms of the as-yet-unknown velocity at the orifice opening.

The solution obtained for each region is capable of cancelling all disturbances on the confining wall. Furthermore, the two solutions are matched kinematically at the opening, since they satisfy the same velocity conditions at $z = d$. However, the solutions have been obtained without accounting for the compatibility of the shear stress and the pressure field across the plane of the opening. A unique solution for f and g can, therefore, be obtained by matching the normal and tangential components of the stress tensor at the interface between the two regions. It can be shown (Dagan, Weinbaum & Pfeffer 1982) that the dynamic condition of matching the stress tensor (2.19) can be satisfied if the pressure and its gradient are matched at $z = d$. Namely,

$$P^{\mathrm{I}}(R, d) = P^{\mathrm{II}}(R, d), \quad \frac{\partial P^{\mathrm{I}}}{\partial z}(R, d) = \frac{\partial P^{\mathrm{II}}}{\partial z}(R, d). \tag{2.25a, b}$$

The general expression for the pressure field in each region can be determined by integrating the creeping-motion equations (2.4) with the appropriate stream-function representation. For the half-space containing the sphere the resulting equation is

$$P^{\mathrm{I}}(R, z) = 2 \int_0^\infty \omega J_0(\omega R) B_1(\omega) e^{\omega z}\, d\omega + 2 \sum_{n=2}^{\infty} D_n \frac{2n-3}{n} \frac{P_{n-1}(\xi)}{r^n} + P_{-\infty}, \tag{2.26}$$

and for the infinite half-space $z \geqslant d$

$$P^{\mathrm{II}}(R, z) = 2 \int_0^\infty \omega J_0(\omega R) B_2(\omega) e^{-\omega z}\, d\omega + P_\infty, \tag{2.27}$$

where $P_{-\infty}$ and P_∞ are the uniform pressures prescribed at $z \to -\infty$ and $z \to \infty$ respectively.

Introducing $B_1(\omega)$ and $B_2(\omega)$ (given in the appendix) into equations (2.26) and (2.27), the pressure-matching conditions (2.25) yield the relations

$$\int_0^\infty \omega^2 J_0(\omega R) \left[\int_0^1 f(t) J_0(\omega t)\, dt \right] d\omega = F^*(R) \quad (0 \leqslant R \leqslant 1), \tag{2.28a}$$

$$\int_0^\infty \omega^3 J_0(\omega R) \left[\int_0^1 g(t) J_1(\omega t)\, dt \right] d\omega = G^*(R) \quad (0 \leqslant R \leqslant 1), \tag{2.28b}$$

where

$$F^*(R) = \frac{1}{2}\int_0^\infty \left\{ \sum_{n=0}^{\infty} B_n [B_n^*(\omega, d) + B_n^{**}(\omega, d)] + D_n [D_n^*(\omega, d) + D_n^{**}(\omega, d)] \right\} \omega^2 J_0(\omega R)\, d\omega$$
$$+ \frac{1}{2} \sum_{n=2}^{\infty} D_n \frac{2n-3}{n} B_{n-1}''(R, d) + \tfrac{1}{4}\Delta P, \tag{2.29a}$$

$$G^*(R) = -\frac{1}{2}\int_0^\infty \left\{ \sum_{n=2}^{\infty} B_n [B_n^*(\omega, d) + B_n^{**}(\omega, d)] + D_n [D_n^*(\omega, d) + D_n^{**}(\omega, d)] \right\} \omega^3 J_0(\omega R)\, d\omega$$
$$+ \frac{1}{2} \sum_{n=2}^{\infty} D_n (2n-3) B_n''(R, d). \tag{2.29b}$$

B_n^*, B_n^{**}, D_n^*, D_n^{**} are given by (A 5), and ΔP is the pressure drop across the orifice, defined by

$$\Delta P = P_{-\infty} - P_\infty \geqslant 0. \tag{2.30}$$

The integral equation (2.28) can be solved for the f and g functions as follows. Defining the new functions

$$f^*(\omega) = \omega \int_0^1 f(t) J_0(\omega t)\, dt, \tag{2.31a}$$

$$g^*(\omega) = \omega^2 \int_0^1 g(t) J_1(\omega t)\, dt, \tag{2.31b}$$

and noting that

$$\int_0^\infty \begin{Bmatrix} f^*(\omega) \\ g^*(\omega) \end{Bmatrix} J_0(\omega R)\, d\omega = 0 \quad (R > 1), \tag{2.32a, b}$$

one obtains two sets of dual integral equations. Using the definition (2.31), one finds that (2.28a) and (2.32a) comprise the set for the function $f^*(\omega)$, while (2.28b) and (2.32b) define the second set for $g^*(\omega)$.

The solution for a dual integral equation of this form is given by Tranter (1951):

$$\begin{Bmatrix} f^*(\omega) \\ g^*(\omega) \end{Bmatrix} = \frac{2}{\pi} \int_0^1 dt \sin \omega t \int_0^t ds \frac{s}{(t^2 - s^2)^{\frac{1}{2}}} \begin{Bmatrix} F^*(s) \\ G^*(s) \end{Bmatrix}. \tag{2.33}$$

The right-hand side in (2.33) is further simplified (see appendix), and the resulting expressions (A 13) are substituted back into (2.22). After considerable algebraic manipulations the velocity components are obtained in the form

$$u_R^{\mathrm{I}} = \sum_{n=2}^{\infty} \left\{ B_n \left[\beta_n'(R, z) + \frac{2}{\pi} \int_0^1 \beta_n^*(R, z, t)\, dt \right] + D_n \left[\delta_n'(R, z) + \frac{2}{\pi} \int_0^1 \delta_n^*(R, z, t)\, dt \right] \right\}$$
$$- \frac{\Delta P}{2\pi} (z - d) H'(R, x), \tag{2.34a}$$

$$u_z^{\mathrm{I}} = \sum_{n=2}^{\infty} \left\{ B_n \left[\beta_n''(R, z) + \frac{2}{\pi} \int_0^1 \beta_n^{**}(R, z, t)\, dt \right] + D_n \left[\delta_n''(R, z) + \frac{2}{\pi} \int_0^1 \delta_n^{**}(R, z, t)\, dt \right] \right\}$$
$$+ \frac{\Delta P}{2\pi} H''(R, x), \tag{2.34b}$$

where $x = z - d$, and the remaining functions (β_n^*, β_n^{**}, δ_n^*, δ_n^{**}, H' and H'') are defined in the appendix.

The solution for the velocity field (2.34) both satisfies the no-slip boundary conditions

on the orifice wall and provides an exact solution for the velocity at the orifice opening. This solution still incorporates the unknown coefficients B_n and D_n, which must be determined from the remaining no-slip boundary conditions on the surface of the sphere. The definite integrals in (2.34) must be performed numerically with special consideration given to the limit as t approaches zero.

On the surface of the sphere, the solution must satisfy the following no-slip boundary conditions:

$$u_R = 0, \quad u_z^{\mathrm{I}} = V, \tag{2.35a, b}$$

where V is the translatory uniform sphere velocity shown in figure 1. Application of these boundary conditions on the surface of the sphere, $r = a$, is accomplished by utilizing the collocation technique first presented by Gluckman *et al.* (1971), and more recently used by Ganatos *et al.* (1980) for the motion of a sphere perpendicular to two plane-parallel walls.

To satisfy the boundary conditions (2.35) exactly on the surface $r = a$ would require the solution of the entire infinite arrays of the unknown spherical coefficients B_n and D_n. Instead, the collocation technique satisfies the boundary conditions at a finite number of discrete points on the sphere's generating arc and truncates the infinite series into a finite one. The two sets of unknown coefficients in each term of the series in (2.34) permit one to satisfy the exact no-slip boundary conditions at one discrete point on the sphere surface. Thus, if the spherical boundary is approximated by satisfying conditions (2.35) at M discrete points on its generating arc, the infinite series in (2.34) is truncated after M terms, resulting in a set of $2M$ simultaneous linear algebraic equations which can be solved for the $2M$ unknown coefficients B_n and D_n by any standard matrix-reduction technique. The accuracy of the truncation technique can be improved by increasing the order M of the truncation. Clearly, as $M \to \infty$ the truncation error vanishes and the overall accuracy of the solution depends only on the accuracy of the numerical integration required in evaluating the matrix elements.

The force exerted by the fluid on the sphere is shown in Happel & Brenner (1973, p. 115) to be

$$F = \pi \int_0^{\pi} r^3 \sin^3\theta \frac{\partial}{\partial r}\left[\frac{D^2\psi}{r^2\sin^2\theta}\right] r\, d\theta. \tag{2.36}$$

Application of this operator and the orthogonality properties of the Gegenbauer function (2.8)–(2.10) results in the simple relation

$$F = 4\pi D_2. \tag{2.37}$$

The drag force can be expressed in terms of two drag coefficient factors $\lambda^{(V)}$ and $\lambda^{(U_0)}$. $\lambda^{(V)}$ describes the case of a sphere translating with velocity V toward the orifice along its centre line in an otherwise quiescent fluid ($\Delta P = 0$), and $\lambda^{(U_0)}$ describes the flow through an orifice past a stationary sphere ($V = 0$).

For a sphere moving with velocity V, the drag force can be written as

$$F = 4\pi D_2^{(V)} = 6\pi a V \lambda^{(V)}, \tag{2.38a}$$

and hence

$$\lambda^{(V)} = \frac{D_2^{(V)}}{1{\cdot}5aV}. \tag{2.38b}$$

Here $\lambda^{(V)}$ represents the ratio of the drag force acting on the sphere in the presence of the confining boundary to the force exhibited under the same conditions in unbounded fluid.

In the case of flow past a stationary sphere, the drag force is given by

$$F = 4\pi D_2^{(U_0)} = 6\pi a U_0 \lambda^{(U_0)}, \tag{2.39a}$$

and hence

$$\lambda^{(U_0)} = \frac{D_2^{(U_0)}}{1{\cdot}5aU_0}, \tag{2.39b}$$

where U_0 is the centre-line fluid velocity in the plane of the orifice in the absence of the sphere and $\lambda^{(U_0)}$ represents the ratio of F to the drag force acting on a stationary sphere in an infinite fluid of uniform velocity U_0.

In the general case, where both the fluid and the sphere are in motion, the linearity of the equation allows one to write the net drag force as the sum of the forces discussed above, i.e.

$$F = 4\pi D_2 = 4\pi[D_2^{(V)} + D_2^{(U_0)}], \tag{2.40a}$$

$$F = 6\pi a[V\lambda^{(V)} + U_0\lambda^{(U_0)}]. \tag{2.40b}$$

3. Solutions for the axisymmetric motion of a sphere towards an orifice in quiescent fluid

The solutions for the motion of a sphere towards an orifice through an otherwise quiescent fluid will be presented in this section together with a detailed description of the convergence characteristics of the collocation technique. The results obtained by the present method for the limiting case as $a \to \infty$ will be compared with the exact solution of Brenner (1961) for translation of a sphere perpendicular to a plane wall.

The system of linear algebraic equations to be solved for B_n and D_n is constructed from (2.34) and the boundary conditions (2.35) with $\Delta P = 0$. When the sphere is moving toward a solid wall ($b' = 0$, $a \to \infty$) the system is easily modified by using (2.22) with $f(R) = 0$ and $g(R) = 0$.

In general, there are many schemes which may be used to select the boundary points on the surface of the sphere to satisfy the no-slip boundary conditions. Two different schemes, which were successfully employed by Leichtberg, Pfeffer & Weinbaum (1976) for the problem of flow past a chain of spheres and by Leichtberg, Weinbaum, Pfeffer & Gluckman (1976) for two closely spaced adjacent spheres in a chain will be examined in detail.

The most accurate lowest-truncation solution for the drag force is obtained by using one boundary point at $\theta = \frac{1}{2}\pi$ on the sphere's generating arc. This point is of great importance since it defines the projected area of the sphere normal to the direction of motion. However, an examination of the system of linear algebraic equations shows that for $\theta = \frac{1}{2}\pi$ the coefficient matrix in (2.34) is singular. In order to overcome this difficulty, the top point $\theta = \frac{1}{2}\pi$ is replaced by two closely spaced adjacent points $\theta = \frac{1}{2}\pi \pm \delta$, where the optimum value of δ is determined by considering a set of solutions for various sphere-to-pore spacings in which the boundary conditions are satisfied only at the top two points for decreasing values of δ. Furthermore, in order to examine the dependence of δ on the ratio of sphere-to-pore diameter the solutions are computed for three different values of a. Consequently, the largest value of δ for

(*a*) $a = 1{\cdot}0$

δ	$\alpha = 0{\cdot}5$, $\frac{d}{a} = 1{\cdot}13$	$\alpha = 1{\cdot}0$, $\frac{d}{a} = 1{\cdot}54$	$\alpha = 2{\cdot}0$, $\frac{d}{a} = 3{\cdot}76$	$\alpha = 3{\cdot}0$, $\frac{d}{a} = 10{\cdot}1$
10°	−2·2272	−1·9432	−1·3862	−1·1247
1°	−2·2160	−1·9353	−1·3855	−1·1246
0·1°	−2·2159	−1·9353	−1·3855	−1·1246
0·01°	−2·2159	−1·9353	−1·3855	−1·1246

(*b*) $a = 10$

δ	$\alpha = 0{\cdot}5$, $\frac{d}{a} = 1{\cdot}13$	$\alpha = 1{\cdot}0$, $\frac{d}{a} = 1{\cdot}54$	$\alpha = 2{\cdot}0$, $\frac{d}{a} = 3{\cdot}76$	$\alpha = 3{\cdot}0$, $\frac{d}{a} = 10{\cdot}1$
10°	−3·5647	−2·5239	−1·4038	−1·1249
1°	−3·4857	−2·4988	−1·4030	−1·1249
0·1°	−3·4849	−2·4986	−1·4030	−1·1249
0·01°	−3·4849	−2·4986	−1·4030	−1·1249

(*c*) $a \to \infty$, $b' = 0$

δ	$\alpha = 0{\cdot}5$, $\frac{d}{a} = 1{\cdot}13$	$\alpha = 1{\cdot}0$, $\frac{d}{a} = 1{\cdot}54$	$\alpha = 2{\cdot}0$, $\frac{d}{a} = 3{\cdot}76$	$\alpha = 3{\cdot}0$, $\frac{d}{a} = 10{\cdot}1$
10°	−3·5674	−2·5251	−1·4039	−1·1249
1°	−3·4885	−2·5000	−1·4030	−1·1249
0·1°	−3·4877	−2·4998	−1·4030	−1·1249
0·01°	−3·4877	−2·4997	−1·4030	−1·1249
0·001°	−3·4877	−2·4997	−1·4030	−1·1249

TABLE 1. Drag-correction factor for a sphere translating axisymmetrically towards an orifice in quiescent fluid; $M = 2$. Convergence test for δ.

which convergence to five significant figures is obtained was selected. These solutions are presented in table 1. The parameter α used in the table is given in terms of the ratio of the dimensionless sphere radius a to the dimensionless distance d by the relationship $\alpha = \operatorname{arcosh}(d/a)$. Table 1 indicates that the rate of convergence of the drag correction factor $\lambda^{(F)}$ is reduced greatly with decreasing α and when $b' = 0$. Convergence to five significant figures for all spacings and sphere radii is achieved when $\delta \leqslant 0{\cdot}01°$. Therefore δ is chosen as $0{\cdot}01°$.

Additional boundary points are selected as mirror-image pairs about the cross-section $\theta = \frac{1}{2}\pi$ in order to maintain the geometrical symmetry of the boundary about this plane. In the first scheme tested the boundary points were selected by dividing the half-arc into equal segments. That is, for an even order of truncation M, the boundary points are defined by $\theta_i = i(180°/M)$ where $i = 1, 2, \ldots, M-1$, with the top point $\theta = 90°$ replaced by the doublet $89{\cdot}99°$ and $90{\cdot}01°$. Using this scheme, solutions for $\lambda^{(F)}$ were obtained for the case of a sphere approaching a solid plane wall ($b' = 0$), for various values of the spacing parameter α, by increasing M until the convergence to five significant digits is achieved. The results, presented in table 2, are compared with the exact solution of Brenner (1961) and are found to be in perfect agreement for the desired accuracy. The rate of convergence is rapid for large values of α and deteriorates monotonically as the distance between the sphere and the wall decreases.

M	$\alpha = 0{\cdot}5$, $\frac{d}{a} = 1{\cdot}13$	$\alpha = 1{\cdot}0$, $\frac{d}{a} = 1{\cdot}54$	$\alpha = 1{\cdot}5$, $\frac{d}{a} = 2{\cdot}35$	$\alpha = 2{\cdot}0$, $\frac{d}{a} = 3{\cdot}76$	$\alpha = 2{\cdot}5$, $\frac{d}{a} = 6{\cdot}13$	$\alpha = 3{\cdot}0$, $\frac{d}{a} = 10{\cdot}1$
2	−3·4877	−2·4997	−1·7728	−1·4030	−1·2202	−1·1249
4	−6·3569	−2·9842	−1·8359	−1·4128	−1·2220	−1·1252
6	−7·8347	−3·0309	−1·8374	−1·4129	−1·2220	−1·1252
8	−8·6423	−3·0356	−1·8375	−1·4129		
10	−9·0189	−3·0360	−1·8375			
12	−9·1693	−3·0361				
14	−9·2237	−3·0361				
16	−9·2424					
18	−9·2486					
20	−9·2507					
22	−9·2514					
24	−9·2516					
26	−9·2517					
28	−9·2518					
30	−9·2518					
*	−9·2518	−3·0361	−1·8375	−1·4129	−1·2220	−1·1252

* Exact solution (Brenner 1961)

TABLE 2. Convergence of $\lambda^{(V)}$ for a sphere translating perpendicular to an infinite plane wall; $b' = 0$

A second scheme for selection of boundary points, tested for the same flow conditions, includes the points $\theta = 0$ and $\theta = \pi$. These points are of great importance when the sphere is located adjacent to the wall since they define the gap between the sphere and the plane at $z = d$. As in the case when $\theta = \frac{1}{2}\pi$, the coefficient matrix (2.34) becomes singular when $\theta = 0$ or π. A similar procedure to that used for the $\theta = \frac{1}{2}\pi$ point is employed to overcome this obstacle. Using $M = 4$ with $\theta = \delta$, $\frac{1}{2}\pi \pm \delta$, $\pi - \delta$, solutions are obtained for various values of δ, α and a. The results are presented in table 3, indicating clearly that $\lambda^{(V)}$ converges to five significant figures for all values of α and a when $\delta \leqslant 0{\cdot}01$, with the slowest convergence rate exhibited when $b' = 0$. Selection of additional points is done in pairs as before. An even number of points M are given by $\theta = (i-1)(180°/(M-2))$ where $i = 1, 2, \ldots, M-1$, and the points $\theta = 0$, 90°, 180° are replaced by $\theta = 0{\cdot}01°$, 89·99°, 90·01°, 189·99° respectively. Solutions obtained for a sphere moving perpendicular to a plane wall for various spacings are presented in table 4 and compared with the exact solution. The solutions obtained by this method converge somewhat faster than those obtained by the previous scheme, shown in table 2. At the distance of closest approach, $\alpha = 0{\cdot}5$, the use of the current scheme yields convergence to five significant digits with 24 boundary points, while the first scheme achieves the same accuracy with 28 points. In view of these tests, the second scheme is seen to provide more rapid convergence and will therefore be used to determine $\lambda^{(V)}$ for various orifice diameters.

Before presenting these results, the effect of the ratio of the sphere-to-pore diameter on the rate of convergence is examined. Since the spherical solution in (2.34) must cancel the disturbance generated at the orifice opening as well, the rate of convergence is expected to deteriorate as the ratio of sphere-to-orifice diameter increases. Solutions were computed for various values of a and d/a with increasing number of boundary

(*a*) $a = 1{\cdot}0$

δ	$\alpha = 0{\cdot}5$, $\frac{d}{a} = 1{\cdot}13$	$\alpha = 1{\cdot}0$, $\frac{d}{a} = 1{\cdot}54$	$\alpha = 2{\cdot}0$, $\frac{d}{a} = 3{\cdot}76$	$\alpha = 3{\cdot}0$, $\frac{d}{a} = 10{\cdot}1$
10°	−2·3084	−2·0026	−1·3870	−1·1247
1°	−2·3016	−1·9983	−1·3864	−1·1246
0·1°	−2·3015	−1·9983	−1·3864	−1·1246
0·01°	−2·3015	−1·9983	−1·3864	−1·1246

(*b*) $a = 10$

δ	$\alpha = 0{\cdot}5$, $\frac{d}{a} = 1{\cdot}13$	$\alpha = 1{\cdot}0$, $\frac{d}{a} = 1{\cdot}54$	$\alpha = 2{\cdot}0$, $\frac{d}{a} = 3{\cdot}76$	$\alpha = 3{\cdot}0$, $\frac{d}{a} = 10{\cdot}1$
10°	−3·5654	−2·5240	−1·4038	−1·1249
1°	−3·4866	−2·4990	−1·4030	−1·1249
0·1°	−3·4859	−2·4987	−1·4030	−1·1249
0·01°	−3·4859	−2·4987	−1·4030	−1·1249

(*c*) $a \to \infty$, $b' = 0$

δ	$\alpha = 0{\cdot}5$, $\frac{d}{a} = 1{\cdot}13$	$\alpha = 1{\cdot}0$, $\frac{d}{a} = 1{\cdot}54$	$\alpha = 2{\cdot}0$, $\frac{d}{a} = 3{\cdot}76$	$\alpha = 3{\cdot}0$, $\frac{d}{a} = 10{\cdot}1$
10°	−20·434	−3·1592	−1·4131	−1·1252
1°	−33·195	−3·1948	−1·4132	−1·1252
0·1°	−33·407	−3·1952	−1·4132	−1·1252
0·01°	−33·409	−3·1952	−1·4132	−1·1252
0·001°	−33·409	−3·1952	−1·4132	−1·1252

TABLE 3. Drag-correction factor for a sphere translating axisymmetrically towards an orifice in quiescent fluid; $M = 4$. Convergence tests for δ.

M	$\alpha = 0{\cdot}5$, $\frac{d}{a} = 1{\cdot}13$	$\alpha = 1{\cdot}0$, $\frac{d}{a} = 1{\cdot}54$	$\alpha = 1{\cdot}5$, $\frac{d}{a} = 2{\cdot}35$	$\alpha = 2{\cdot}0$, $\frac{d}{a} = 3{\cdot}76$	$\alpha = 2{\cdot}5$, $\frac{d}{a} = 6{\cdot}13$	$\alpha = 3{\cdot}0$, $\frac{d}{a} = 10{\cdot}1$
4	−33·409	−3·1952	−1·8428	−1·4132	−1·2220	−1·1252
6	−14·902	−3·0399	−1·8374	−1·4129	−1·2220	−1·1252
8	−9·8323	−3·0360	−1·8375	−1·4129		
10	−9·3260	−3·0361	−1·8375			
12	−9·2603	−3·0361				
14	−9·2513					
16	−9·2510					
18	−9·2515					
20	−9·2517					
22	−9·2517					
24	−9·2518					
26	−9·2518					
*	−9·2518	−3·0361	−1·8375	−1·4129	−1·2220	−1·1252

* Exact solution (Brenner 1961)

TABLE 4. Convergence of $\lambda^{(V)}$ for a sphere translating perpendicular to an infinite plane wall with boundary points placed near $\theta = 0, \pi$; $b' = 0$

$\frac{d}{a}$	M	$a = 0{\cdot}1$	$a = 0{\cdot}5$	$a = 1{\cdot}0$	$a = 10$
5·0	4	−1·0532	−1·2508	−1·2795	−1·2851
	6	−1·0532	−1·2509	−1·2795	−1·2851
	8	−1·0532	−1·2509	−1·2795	−1·2851
2·0	6	−1·0505	−1·3918	−1·8066	−2·1248
	8	−1·0505	−1·3919	−1·8058	−2·1248
	10	−1·0505	−1·3919	−1·8058	−2·1248
1·5	8	−1·0504	−1·3882	−2·0335	−3·1981
	10	−1·0504	−1·3882	−2·0334	−3·1983
	12	−1·0504	−1·3882	−2·0334	−3·1983
1·1	16	−1·0504	−1·3777	−2·2867	−10·593
	18	−1·0504	−1·3777	−2·2867	−10·590
	20	−1·0504	−1·3777	−2·2867	−10·566
	22	—	—	—	−10·543
	24	—	—	—	−10·527
	26	—	—	—	−10·517
	28	—	—	—	−10·512
	30	—	—	—	−10·511

TABLE 5. Convergence of $\lambda^{(V)}$ for various sphere radii a and sphere-to-orifice spacings d/a

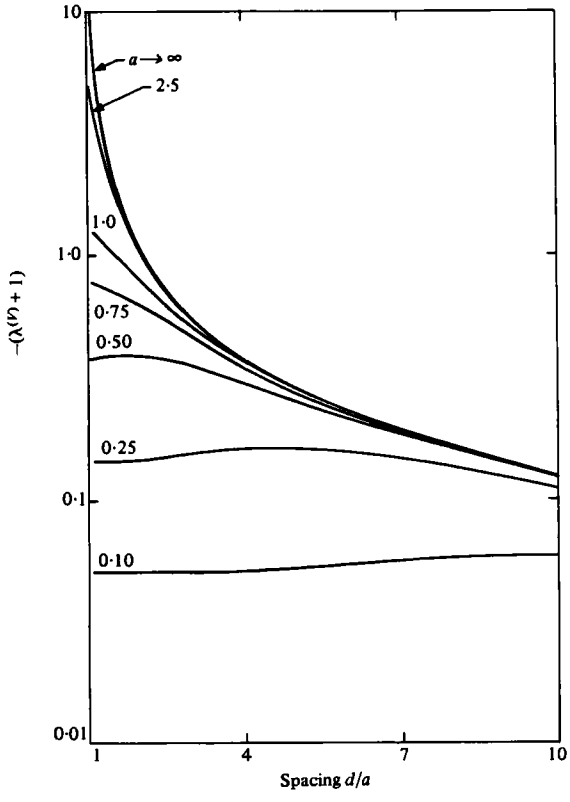

FIGURE 2. Drag on a sphere translating axisymmetrically towards an orifice.

d/a	$a = 0{\cdot}10$	$a = 0{\cdot}25$	$a = 0{\cdot}50$	$a = 0{\cdot}75$	$a = 1{\cdot}00$	$a = 2{\cdot}50$	$a = 5{\cdot}00$	$a = 7{\cdot}50$	$a = 10{\cdot}0$
1·1	−1·0503	−1·1412	−1·3777	−1·7666	−2·2867	−5·89	−8·94	−9·99	−10·5
1·25	−1·0502	−1·1419	−1·3819	−1·7497	−2·1807	−4·0355	−4·9183	−5·1532	−5·2340
1·5	−1·0504	−1·1433	−1·3882	−1·7164	−2·0334	−2·9207	−3·1535	−3·1889	−3·1983
2·0	−1·0505	−1·1475	−1·3919	−1·6348	−1·8058	−2·0857	−2·1200	−2·1239	−2·1248
3·0	−1·0510	−1·1579	−1·3581	−1·4679	−1·5168	−1·5649	−1·5687	−1·5690	−1·5691
4·0	−1·0519	−1·1637	−1·3019	−1·3491	−1·3655	−1·3791	−1·3801	−1·3802	−1·3802
5·0	−1·0532	−1·1617	−1·2509	−1·2728	−1·2795	−1·2847	−1·2850	−1·2851	−1·2851
6·0	−1·0549	−1·1541	−1·2110	−1·2222	−1·2254	−1·2277	−1·2279	−1·2279	−1·2279
8·0	−1·0579	−1·1328	−1·1571	−1·1608	−1·1617	−1·1624	−1·1625	−1·1625	−1·1625
10·0	−1·0596	−1·1125	−1·1240	−1·1255	−1·1262	−1·1262	−1·1262	−1·1262	−1·1262

TABLE 6. Drag-correction factor $\lambda^{(V)}$ for a sphere translating axisymmetrically towards an orifice for various sphere radii a and sphere-to-orifice spacings d/a

points, starting with the minimum value of M from table 4 which yields convergence to four significant digits. Examination of these solutions, shown in table 5, indicates that the pore size has little effect on the rate of convergence except when a is large and the sphere is adjacent to the orifice. The slow convergence for the case $a = 10$ and $d/a = 1{\cdot}1$ is due mainly to the high velocity gradient in the gap between the sphere and the wall. This necessitates choosing a high concentration of boundary points on the section of the sphere surface closest to the orifice wall. Therefore, for large values of a and small values of d/a, when convergence is slow and computation time is prohibitively long, the accuracy will be reduced to three significant digits.

Final results for $\lambda^{(V)}$ for various dimensionless sphere radius and sphere-to-wall spacings are presented in table 6. The solutions are plotted in figure 2 together with the exact solution for the case of motion perpendicular to an infinite plane wall, corresponding to the limiting case when $a \to \infty$. An interesting result, observed in figure 2, is that the drag on a sphere whose diameter is smaller than that of the orifice decreases when the sphere is close to the orifice, with a relative minimum value at the centre of the opening. This effect is due to the decreasing of the effective wall-interaction area that offers resistance to the motion of a 'small sphere' as it approaches the opening.

4. Solution for the flow through an orifice past a stationary sphere

The results for $\lambda^{(U_0)}$ for the case of flow into an orifice past a stationary sphere are obtained from the solution of the system of linear algebraic equations defined by (2.34) and the boundary conditions (2.35) with $V = 0$.

The collocation technique is employed in a manner similar to that described in §3. The two schemes for selection of boundary points are tested again. The singularity of the coefficient matrix at $\theta = 0, \pi$ is avoided by using the points $\theta = \frac{1}{2}\pi \pm \delta$ for the first scheme and $\theta = \delta$, $\frac{1}{2}\pi \pm \delta$, $\pi - \delta$ for the second scheme and taking the limit $\delta \to 0$ convergence is achieved to the desired number of digits. Again, convergence to five significant digits was achieved for all spacings for $\delta \leqslant 0{\cdot}01°$. Tables presenting the results for these tests are contained in Dagan (1980) and will not be repeated here. In order to test the convergence of the first scheme, solutions are computed for $a = 1$ and for increasing number of boundary points. Based on the results in §3, solutions were not computed for small values of M, when the results are from the final converged value. The procedure was repeated with the second collocation scheme. Comparison of the results, presented in tables 7 and 8, shows no major difference between the two schemes. This behaviour may be explained by the fact that large fluid velocities can be generated in the gap between the sphere and the edge of the orifice rather than in the front of the sphere, where the gap between the sphere and the orifice plane is smaller. Nevertheless, the second scheme is chosen in further computations for the sake of consistency.

The effect of the ratio of space-to-pore diameter on the rate of convergence was tested and is presented in table 9. Examination of these solutions indicates that convergence deteriorates for large values of a and small spacing. For $a = 10$ and $d = 1{\cdot}1$ the results converge to only three significant digits with 30 boundary points.

Solutions for $\lambda^{(U_0)}$ for various values of a and d/a are plotted in figure 3 and are presented, for reference, in table 10. Figure 3 indicates that for a fixed pressure drop

M	$\frac{d}{a} = 1{\cdot}1$	$\frac{d}{a} = 1{\cdot}5$	$\frac{d}{a} = 2{\cdot}0$	$\frac{d}{a} = 5{\cdot}0$	$\frac{d}{a} = 10{\cdot}0$
4	—	—	—	—	0·011092
6	—	—	0·32709	0·048593	0·011094
8	—	0·48351	0·32756	0·048597	0·011094
10	—	0·48326	0·32755	0·048597	
12	—	0·48321	0·32754		
14	—	0·48320	0·32754		
16	0·64020	0·48320			
18	0·64018				
20	0·64018				

TABLE 7. Convergence of $\lambda^{(U_0)}$ for the flow through an orifice past a stationary sphere at various sphere-to-orifice spacings d/a; $a = 1{\cdot}0$

M	$\frac{d}{a} = 1{\cdot}1$	$\frac{d}{a} = 1{\cdot}5$	$\frac{d}{a} = 2{\cdot}0$	$\frac{d}{a} = 5{\cdot}0$	$\frac{d}{a} = 10{\cdot}0$
4	—	—	—	—	0·011102
6	—	—	0·32639	0·048591	0·011094
8	—	0·48302	0·32756	0·048597	0·011094
10	—	0·48315	0·32754	0·048597	
12	—	0·48319	0·32754		
14	—	0·48320			
16	0·64017	0·48320			
18	0·64018				
20	0·64018				

TABLE 8. Convergence of $\lambda^{(U_0)}$ for the flow through an orifice past a stationary sphere at various sphere-to-orifice spacings d/a, with boundary points at $\theta = 0, \pi$; $a = 1{\cdot}0$

$\frac{d}{a}$	M	$a = 0{\cdot}1$	$a = 0{\cdot}5$	$a = 1{\cdot}0$	$a = 10$
5·0	6	0·83796	0·16985	0·048591	0·000507 65
	8	0·83796	0·16986	0·048697	0·000507 74
	10	0·83796	0·16986	0·048597	0·000507 74
2·0	6	1·0036	0·62755	0·32639	0·0057674
	8	1·0036	0·62719	0·32756	0·0056361
	10	1·0036	0·62720	0·32754	0·0056518
	12	—	0·62720	0·32754	0·0056541
	14	—	0·62720	0·32754	0·0056546
	16	—	—	—	0·0056546
1·5	8	1·0206	0·77574	0·48302	0·018657
	10	1·0206	0·77576	0·48315	0·018353
	12	1·0206	0·77576	0·48319	0·018433
	14	—	0·77576	0·48320	0·018465
	16	—	—	0·48320	0·018479
	18	—	—	0·48320	0·018484
1·1	16	1·0310	0·90571	0·64017	0·13261
	18	1·0310	0·90571	0·64018	0·13360
	20	1·0310	0·90571	0·64018	0·13847
	22	—	—	0·64018	0·14294
	24	—	—	—	0·14610
	26	—	—	—	0·14799
	28	—	—	—	0·14882
	30	—	—	—	0·14899

TABLE 9. Convergence of $\lambda^{(U_0)}$ for various sphere radii a and sphere-to-orifice spacings d/a

$\frac{d}{a}$	$a = 0{\cdot}1$	$a = 0{\cdot}25$	$a = 0{\cdot}5$	$a = 0{\cdot}75$	$a = 1{\cdot}0$	$a = 2{\cdot}5$	$a = 5{\cdot}0$	$a = 7{\cdot}5$	$a = 10$
1·1	1·0310	1·0192	0·90571	0·76406	0·64018	0·295	0·191	0·168	0·149
1·25	1·0274	0·99990	0·85661	0·70015	0·57535	0·282	0·159	0·0937	0·0586
1·5	1·0206	0·96446	0·77576	0·60451	0·48320	0·19675	0·0683	0·0323	0·0185
2·0	1·0036	0·88537	0·62720	0·44502	0·32754	0·082813	0·022291	0·010018	0·0056546
3·0	0·95824	0·71899	0·39761	0·23318	0·14785	0·027119	0·0068979	0·0030746	0·0017312
4·0	0·90148	0·56854	0·25386	0·13232	0·079031	0·013477	0·0033973	0·0015122	0·00085101
5·0	0·83796	0·44578	0·16986	0·083373	0·048597	0·0080729	0·0020285	0·00090236	0·00050774
6·0	0·77168	0·35077	0·11976	0·056922	0·032785	0·0053786	0·0013493	0·00060005	0·00033160
8·0	0·64234	0·22494	0·067600	0·031160	0·017752	0·0028792	0·00072118	0·00032064	0·00018038
10·0	0·52797	0·15272	0·043026	0·019566	0·011094	0·0017904	0·00044814	0·00019922	0·00011207

TABLE 10. Drag correction factor $\lambda^{(U_0)}$ for a flow through an orifice past a stationary sphere for various sphere radii a and sphere-to-orifice spacings d/a

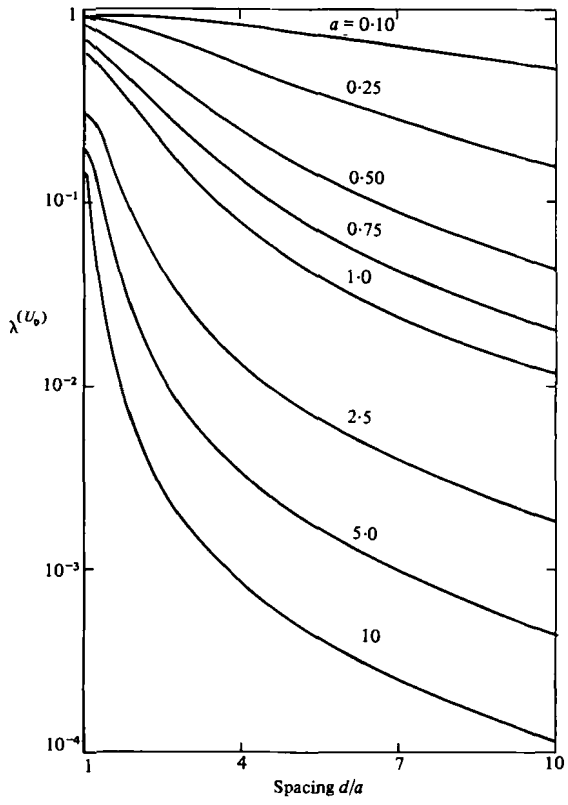

FIGURE 3. Drag on a rigidly held sphere in flow through an orifice.

across the orifice the drag force increases with decreasing spacing for all sphere sizes and approaches a finite value when the sphere touches the plane of the pore. One notes that the drag on the sphere decreases markedly as the sphere size increases for a fixed ΔP. This is a consequence of the reduction of the volume flow through the orifice due to the obstruction of the sphere. The relationship between volume-flow pressure drop and sphere size is examined in §5.

5. Pressure drop across the orifice

The relations between the volumetric flow rate and the pressure drop across the orifice, in the presence of a sphere, can be obtained by integrating the axial velocity u_z^{I} over the area of the orifice opening. The integration can be performed analytically yielding the expression

$$Q = \tfrac{1}{3}\Delta P + 4\sum_{n=2}^{\infty}\frac{B_n}{n}\left[\frac{S_{n-1}(1,d)}{n-1} - C_n(d)\right] + \frac{2D_2}{d^2+1} + 4\sum_{n=3}^{\infty}\left\{D_n\frac{(2n-3)d}{n(n-1)}\left[\frac{S_{n-2}(1,d)}{n-2} - C_{n-1}(d)\right] + D_{n+1}\frac{1}{n^2-1}\left[S_{n-2}(1,d) - (n-2)C_{n-1}(d)\right]\right\}, \tag{5.1}$$

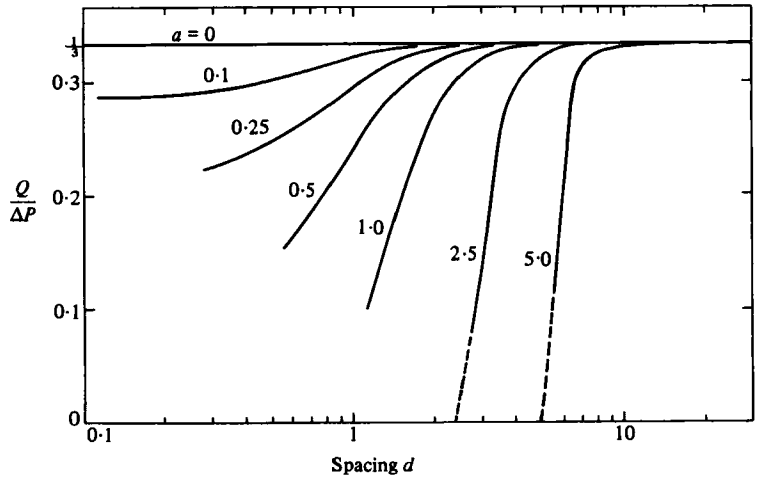

FIGURE 4. Pressure drop across an orifice for flow past a rigidly held sphere. – – – –, extrapolated results.

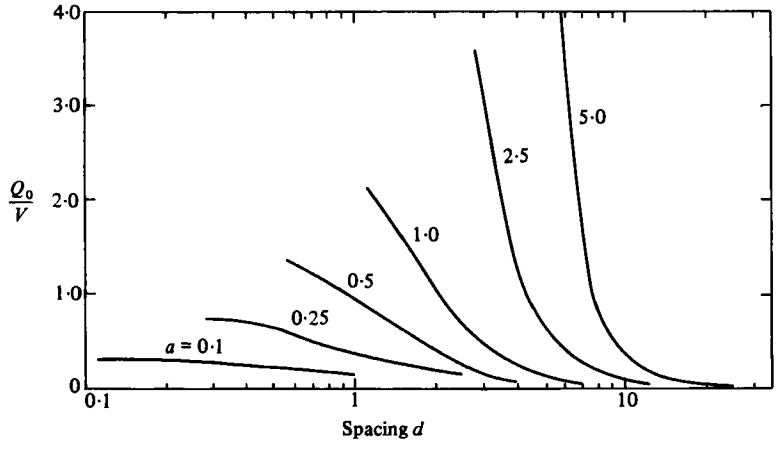

FIGURE 5. Volumetric flow rate through an orifice due to the translatory motion of a sphere.

where Q is the dimensionless volumetric flow rate defined in a similar manner to the stream function in (2.3a). S_n is defined by (A 16a) in the appendix and

$$C_n(d) = \frac{\cos(n \operatorname{arccot} d)}{(1+d^2)^{\frac{1}{2}n}}. \tag{5.2}$$

An important application of (5.1) is the operation of a ball valve in the low-Reynolds-number regime. In this application a ball whose dimensions are larger than the orifice is constrained from moving by a wire at a fixed distance above the orifice.

Clearly, when the sphere is far from the orifice ($d \to \infty$) (5.1) reduces to

$$Q = \tfrac{1}{3}\Delta P, \tag{5.3}$$

which is in agreement with the exact solution for flow through an orifice in the absence of a sphere.

The relationship between Q and ΔP was computed for the case where the sphere is

held rigidly at a prescribed distance from the orifice. These results are presented in figure 4 for various sphere diameters.† Examination of these results indicates that the volumetric flow rate decreases, for a prescribed pressure drop across the orifice, with decreasing spacing. For a sphere of diameter larger than the orifice diameter ($a \geqslant 1$) Q decreases rapidly when $d/a < 2$ and approaches zero when the sphere blocks the orifice entirely. The results for $d/a < 1{\cdot}1$, when the sphere diameter is larger than that of the orifice, are extrapolated and shown by the dashed lines.

In the case of a sphere moving with velocity V towards an orifice in quiescent fluid ($\Delta P = 0$) the volumetric flow rate at the pore opening Q_0 is presented in figure 5. Here, Q_0 increases with increasing sphere size and decreasing distance between the sphere and the orifice.

The total volumetric flow rate through the orifice for the general case when a sphere is moving with velocity V and the pressure drop across the orifice is prescribed by ΔP can be obtained by adding the two distinct contributions given by figures 4 and 5.

6. The axisymmetric motion of a sphere in a flow through an orifice

In this section, a solution for the velocity of a sphere carried by the fluid toward the orifice is presented by combining the axisymmetric solutions for the motion of a sphere in a quiescent fluid and the flow through an orifice past a stationary sphere.

One problem of interest considers a sphere suspended above an orifice in which fluid is being pumped against gravity. The flow rate required to keep the sphere stationary can be determined by setting $V = 0$ in (2.40) and equating F to the force due to gravity. The result is

$$U_0 = -\frac{V_t}{\lambda^{(U_0)}}, \tag{6.1}$$

where V_t is the terminal settling velocity in an infinite medium.

Another application of interest is the motion of a neutrally buoyant sphere carried by the flow toward the pore. In this case we require a zero drag force on the sphere. Equation (2.40) reduces to

$$\frac{V}{U_0} = -\frac{\lambda^{(U_0)}}{\lambda^{(V)}}, \tag{6.2}$$

from which the local sphere velocity V is obtained.

Of particular interest is the slip velocity of the neutrally buoyant sphere, defined by

$$V_{\text{slip}} = V - U, \tag{6.3}$$

where U is the local fluid velocity in the absence of the sphere and can be related to U_0 by

$$\frac{U}{U_0} = (1+d^2)^{-1}; \tag{6.4}$$

hence

$$\frac{V_{\text{slip}}}{U} = -\left[\frac{\lambda^{(U_0)}}{\lambda^{(V)}}(d^2+1)+1\right] \tag{6.5a}$$

or

$$\frac{V}{U} = -\frac{\lambda^{(U_0)}}{\lambda^{(V)}}(d^2+1). \tag{6.5b}$$

† Note that in the subsequent figures the abscissa is d and not d/a. The latter choice will show the curves too close to each other.

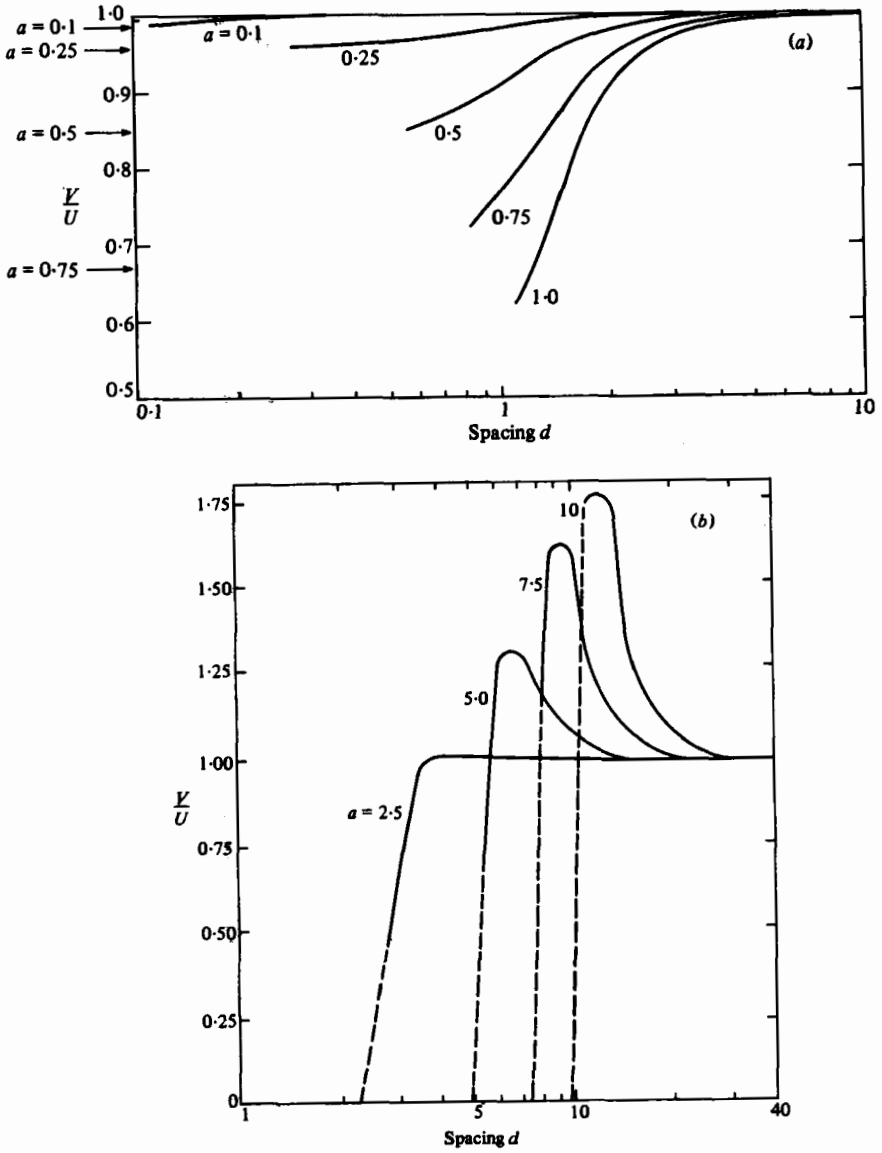

FIGURE 6. (*a*) Velocity of a neutrally buoyant sphere carried by the flow through an orifice; $a \leqslant 1{\cdot}0$. (*b*) Velocity of a neutrally buoyant sphere carried by the flow through an orifice; $a > 1{\cdot}0$; – – – –, extrapolated results.

Equation (6.5*b*) is plotted in figures 6(*a*, *b*). Figure 6(*a*) shows the ratio of the sphere velocity to the undisturbed local fluid velocity for spheres with radius $a \leqslant 1$. The results indicate that the sphere velocity is smaller than the local fluid velocity. These results are compared with the zero-drag velocity of a sphere carried axisymmetrically in an infinite tube (Haberman & Sayre 1958), shown by the arrowheads on the ordinate. Clearly, the present results approach this limiting case and it is easy to extrapolate the zero-drag velocity for a sphere entering a semi-infinite cylindrical pore. In contrast, for spheres larger than the orifice diameter (figure 6*b*) the sphere velocity increases rapidly as the sphere approaches the orifice and then drops sharply

when $d/a < 1{\cdot}25$. This behaviour can be explained by the fact that when the gap between the sphere and the orifice decreases the fluid velocity rises quickly, enhancing the motion of the sphere. With further decrease of the gap width, the blocking of the orifice by the sphere reduces the volumetric flow rate (see figure 4), which in turn retards the sphere motion. The dashed extensions in figure 6(*b*) are extrapolated results for the sphere velocity for small spacings $d/a < 1{\cdot}1$.

Finally, it may be of interest to compare the slip velocity or the ratio V/U with the approximate result one can readily obtain from the widely used Faxen's law (Happel & Brenner 1973) in the form

$$\frac{V}{U} = \left[1 + \frac{3a^3}{(1+d^2)^3}\right]^{-1}. \tag{6.6}$$

Clearly, (6.6) cannot describe the behaviour shown in figure 6(*b*), where $V/U > 1$. It is valid only for $a/d \ll 1$, when the flow field is barely affected by the presence of the sphere. For example, when $d = 1$ and $a = 0{\cdot}1$, $0{\cdot}25$, $0{\cdot}5$, $0{\cdot}75$ the errors in using (6.6) compared with figure 6(*a*) are $0{\cdot}1$, $1{\cdot}4$, $6{\cdot}1$ and $11{\cdot}4\,\%$ respectively.

The calculations for the results presented in this paper were performed on an AMDAHL 470/V6 computer. The bulk of the computation time was used in the numerical integration required for the evaluation of the coefficient matrix. Actual computer execution times were found to be approximately $\frac{1}{7}M^2$ s per run, with increasing execution time for small sphere sizes due to slower evaluation of the integrals in (2.34).

The authors wish to thank the National Science Foundation for supporting this research under grant ENG78–22101, and The City University of New York Computer Center for the use of their facilities. The above work has been performed in partial fulfilment of the requirements for the Ph.D. degree of Z. Dagan from the School of Engineering of The City College of The City University of New York.

Appendix

For the purpose of conciseness some of the mathematical derivations discussed in §2 are given here.

(*a*) *Integration of* (2.21) *and evaluation of* $k_1'(\omega, z)$ *and* $k_1''(\omega, z)$

The integrals in (2.21) can be performed analytically by making use of the integral given by Erdélyi *et al.* (1954, vol. 2, p. 45)

$$\int_0^\infty \frac{x}{(a^2+x^2)^{\frac{1}{2}\mu}} P^\nu_{\mu-1}\left(\frac{a}{(a^2+x^2)^{\frac{1}{2}}}\right) J_\nu(xy)\,dx = \frac{y^{\mu-2}e^{-ay}}{\Gamma(\mu+\nu)} \quad (\mathscr{R}\nu > -1, \mathscr{R}\mu > \tfrac{1}{2}), \tag{A 1}$$

the Legendre-polynomial representation of the Gegenbauer function given by

$$I_n(x) = \frac{P_{n-2}(x) - P_n(x)}{2n-1}, \tag{A 2}$$

and the recurrence relation for Legendre polynomials. Thus, one can show that

$$\int_0^\infty \frac{1}{(t^2+d^2)^{\frac{1}{2}n}} I_{n+1}\left(\frac{d}{(t^2+d^2)^{\frac{1}{2}}}\right) J_1(\omega t)\,dt = \frac{\omega^{n-1}}{(n+1)!} e^{-\omega d}, \tag{A 3a}$$

$$\int_0^\infty \frac{1}{(t^2+d^2)^{\frac{1}{2}(n+2)}} I_{n+1}\left(\frac{d}{(t^2+d^2)^{\frac{1}{2}}}\right) J_1(\omega t)\,dt = \frac{\omega^{n-3}}{(n+1)!}[(2n-1)\,\omega d - n(n-2)]\,e^{-\omega d}, \tag{A 3b}$$

$$\int_0^\infty \frac{t}{(t^2+d^2)^{\frac{1}{2}(n+1)}} P_n\left(\frac{d}{(t^2+d^2)^{\frac{1}{2}}}\right) J_0(\omega t)\,dt = \frac{\omega^{n-1}}{n!}\,e^{-\omega d}, \tag{A 3c}$$

$$\int_0^\infty \frac{t}{(t^2+d^2)^{\frac{1}{2}(n-1)}} P_n\left(\frac{d}{(t^2+d^2)^{\frac{1}{2}}}\right) J_0(\omega t)\,dt = \frac{\omega^{n-3}}{n!}[(2n-1)\,\omega d - (n-1)^2]\,e^{-\omega d}, \tag{A 3d}$$

$$\int_0^\infty \frac{t}{(t^2+d^2)^{\frac{1}{2}(n-1)}} I_n\left(\frac{d}{(t^2+d^2)^{\frac{1}{2}}}\right) J_0(\omega t)\,dt = \frac{\omega^{n-3}}{n!}[(n-1) - \omega d]\,e^{-\omega d}. \tag{A 3e}$$

Utilizing these results in (2.21) yields

$$k_1'(\omega, d) = \sum_{n=2}^{\infty} [B_n B_n^*(\omega, d) + D_n D_n^*(\omega, d)] + \int_0^1 g(t)\, J_1(\omega t)\,dt, \tag{A 4a}$$

$$k_1''(\omega, d) = \sum_{n=2}^{\infty} [B_n B_n^{**}(\omega, d) + D_n D_n^{**}(\omega, d)] + \int_0^1 f(t)\, J_0(\omega t)\,dt, \tag{A 4b}$$

where

$$B_n^*(\omega, d) = \int_0^\infty B_n'(t, d)\, t\, J_1(\omega t)\,dt = \frac{\omega^{n-1}}{n!}\,e^{-\omega d}, \tag{A 5a}$$

$$D_n^*(\omega, d) = \int_0^\infty D_n'(t, d)\, t\, J_1(\omega t)\,dt = \frac{\omega^{n-3}}{n!}[(2n-3)\,\omega d - n(n-2)]\,e^{-\omega d}, \tag{A 5b}$$

$$B_n^{**}(\omega, d) = \int_0^\infty B_n''(t, d)\, t\, J_0(\omega t)\,dt = \frac{\omega^{n-1}}{n!}\,e^{-\omega d}, \tag{A 5c}$$

$$D_n^{**}(\omega, d) = \int_0^\infty D_n''(t, d)\, t J_0(\omega t)\,dt = \frac{\omega^{n-3}}{n!}[(2n-3)\,\omega d - (n-1)\,(n-3)]\,e^{-\omega d}. \tag{A 5d}$$

The functions k_1' and k_1'', in (A 4) and (A 5), evaluated at $z = d$, are expressed in terms of the unknown coefficients B_n and D_n in the spherical solution, and the unknown velocity components f and g at the opening. To obtain the expression for the velocity field, the Fourier functions $A_1(\omega)$ and $B_1(\omega)$ in the expressions for k_1' and k_1'' must be determined. This is accomplished by evaluating (2.14a) and (2.14d) at $z = d$ and equating with (A 4). The resulting equations are then solved for $A_1(\omega)$ and $B_1(\omega)$

$$\begin{aligned} A_1(\omega)\, e^{\omega d} = {} & -\omega d \int_0^1 g(\xi)\, J_1(\omega\xi)\,d\xi + (1+\omega d)\int_0^1 f(\xi)\, J_0(\omega\xi)\,d\xi \\ & - \sum_{n=2}^{\infty} \{B_n[B_n^{**}(\omega, d)\,(1+\omega d) + \omega d B_n^*(\omega, d)] \\ & + D_n[D_n^{**}(\omega, d)\,(1+\omega d) + \omega d D_n^*(\omega, d)]\}, \end{aligned} \tag{A 6}$$

$$\begin{aligned} B_1(\omega)\, e^{\omega d} = {} & \omega\left[\int_0^1 g(\xi)\, J_1(\omega\xi)\,d\xi - \int_0^1 f(\xi)\, J_0(\omega\xi)\,d\xi\right] \\ & + \omega \sum_{n=2}^{\infty} \{B_n[B_n^*(\omega, d) + B_n^{**}(\omega, d)] + D_n[D_n^*(\omega, d) + D_n^{**}(\omega, d)]\}. \end{aligned} \tag{A 7}$$

Equations (A 6) and (A 7) are substituted back into (2.14a, d), yielding the following results:

$$k_1'(\omega,z) = -\left\{[\omega(d-z)-1]\int_0^1 g(t)\,J_1(\omega t)\,dt - \omega(d-z)\int_0^1 f(t)\,J_0(\omega t)\,dt\right\} e^{-\omega(d-z)}$$
$$+\sum_{n=2}^{\infty} B_n\{[1-\omega(d-z)]\,B_n^*(\omega,d) - \omega(d-z)\,B_n^{**}(\omega,d)\}\,e^{-\omega(d-z)}$$
$$+\sum_{n=2}^{\infty} D_n\{[1-\omega(d-z)]\,D_n^*(\omega,d) - \omega(d-z)\,D_n^{**}(\omega,d)\}\,e^{-\omega(d-z)}, \quad \text{(A 8}a\text{)}$$

$$k_1''(\omega,z) = \left\{[1+\omega(d-z)]\int_0^1 f(t)\,J_0(\omega t)\,dt - \omega(d-z)\int_0^1 g(t)\,J_1(\omega t)\,dt\right\} e^{-\omega(d-z)}$$
$$-\sum_{n=2}^{\infty} B_n\{\omega(d-z)\,B_n^*(\omega,d) + [1+\omega(d-z)]\,B_n^{**}(\omega,d)\}\,e^{-\omega(d-z)}$$
$$-\sum_{n=2}^{\infty} D_n\{\omega(d-z)\,D_n^*(\omega,d) + [1+\omega(d-z)]\,D_n^{**}(\omega,d)\}\,e^{-\omega(d-z)}. \quad \text{(A 8}b\text{)}$$

(b) *The functions $A_2(\omega)$ and $B_2(\omega)$*

$$A_2(\omega)\,e^{-\omega d} = (1-\omega d)\int_0^1 f(\xi)\,J_0(\omega\xi)\,d\xi - \omega d\int_0^1 g(\xi)\,J_1(\omega\xi)\,d\xi, \quad \text{(A 9)}$$

$$B_2(\omega)\,e^{-\omega d} = \omega\left[\int_0^1 f(\xi)\,J_0(\omega\xi)\,d\xi + \int_0^1 g(\xi)\,J_1(\omega\xi)\,d\xi\right]. \quad \text{(A 10)}$$

(c) *Simplification of* (2.33)

The functions F^* and G^* are substituted from (2.29) into (2.33), where B_n'' is replaced by its integral transform given in (A 5). The resulting right-hand side of (2.33) consists of triple-integral expressions, of which two integrals can be performed analytically. The middle integral is evaluated first using the result given by Erdélyi *et al.* (1954, vol. 2, p. 7):

$$\int_0^t \frac{s}{(t^2-s^2)^{\frac{1}{2}}}\,J_0(\xi s)\,ds = \frac{1}{\xi}\sin t\xi. \quad \text{(A 11)}$$

Then the improper inner integral is determined using the basic relations (Erdélyi *et al.* 1954, vol. 1, p. 152)

$$\int_0^\infty \sin\xi t\,\xi^{n-1}e^{-\xi d}\,d\xi = \frac{\Gamma(n)}{(d^2+t^2)^{\frac{1}{2}n}}\sin\left(n\arctan = \frac{t}{d}\right) \quad (\mathscr{R}n > -1,\ \mathscr{R}d > |\mathscr{I}t|). \quad \text{(A 12)}$$

The resulting expressions for f^* and g^* are

$$f^*(\omega) = \frac{\Delta P}{2\pi\omega}\left(\frac{\sin\omega}{\omega} - \cos\omega\right) + \sum_{n=2}^{\infty}\left\{B_n F_{n+1}(\omega,d) + D_n\left[\frac{2n-3}{n}F_n(\omega,d) - \frac{n-3}{n}F_{n-1}(\omega,d)\right]\right\}, \quad \text{(A 13}a\text{)}$$

$$g^*(\omega) = -\sum_{n=2}^{\infty}\{B_n(n+1)\,F_{n+2}(\omega,d) + D_n[(2n-3)\,dF_{n+1}(\omega,d) - (n-2)\,F_n(\omega,d)]\}, \quad \text{(A 13}b\text{)}$$

where F_n is the remaining outer integral given by

$$F_n(\omega, d) = \frac{2}{\pi}\int_0^1 \sin \omega t \frac{\sin (n \arctan t/d)}{(t^2+d^2)^{\frac{1}{2}n}}\, dt. \tag{A 14}$$

Equations (A 13) and (A 14) provide the solutions for f^* and g^* in terms of the unknown spherical coefficients B_n and D_n. Utilizing these results and the definitions of f^* and g^* given by (2.31), one can determine the functions f and g using Hankel's inversion formulae. One can also substitute the f^* and g^* functions directly in (2.22) to obtain the expression for the velocity field in the region $z \leqslant d$, in terms of the unknown coefficients B_n and D_n.

(*d*) *Definition of the functions in* (2.34)

$$\beta_n^*(R, z, t) = (n+1)\, S_{n+2}(t, d)\, [k_1^{-1}(R, x, t) - x k_1^0(R, x, t)] - x S_{n+1}(t, d)\, k_1^1(R, x, t), \tag{A 15a}$$

$$\delta_n^*(R, z, t) = [k_1^{-1}(R, x, t) - x k_1^0(R, x, t)]\, [(2n-3)\, d S_{n+1}(t, d) - (n-2)\, S_n(t, d)] + \frac{x}{n} k_1^1(R, x, t)\, [(n-3)\, S_{n-1}(t, d) - (2n-3)\, d S_n(t, d)], \tag{A 15b}$$

$$H'(R, x) = \int_0^\infty \left(\frac{\sin \omega}{\omega} - \cos \omega\right) J_1(\omega R)\, e^{-\omega x}\, d\omega, \tag{A 15c}$$

$$\beta_n^{**}(R, z, t) = S_{n+1}(t, d)\, [k_0^0(R, x, t) + x k_0^1(R, x, t)] + x(n+1)\, S_{n+2}(t, d)\, k_0^0(R, x, t)], \tag{A 15d}$$

$$\delta_n^{**}(R, z, t) = [k_0^0(R, x, t) + x k_0^1(R, x, t)] \left[\frac{2n-3}{n} d S_n(t, d) - \frac{n-3}{n} S_{n-1}(t, d)\right] + x k_0^0(R, x, t)\, [(2n-3)\, d S_{n+1}(t, d) - (n-2)\, S_n(t, d)], \tag{A 15e}$$

$$H''(R, x) = \int_0^\infty \left(\frac{1}{\omega} + x\right) \left(\frac{\sin \omega}{\omega} - \cos \omega\right) J_0(\omega R)\, e^{-\omega x}\, d\omega, \tag{A 15f}$$

where

$$S_n(t, d) = (d^2+t^2)^{-\frac{1}{2}n} \sin \left(n \arctan \frac{t}{d}\right), \tag{A 16a}$$

$$k_\nu^\mu(R, x, t) = \int_0^\infty \omega^\mu J_\nu(\omega R)\, e^{-\omega x} \sin \omega t\, d\omega. \tag{A 16b}$$

The integrals k_ν^μ in (A 15) can be evaluated analytically by making use of the basic result (Erdélyi *et al.* 1954, vol. 1, p. 101)

$$k_1^{-1}(R, x, t) = \frac{t}{R}(1-h), \tag{A 17a}$$

where h is a positive root of the algebraic equation

$$t^2 = \frac{R^2}{1-h^2} - \frac{x^2}{h^2}. \tag{A 17b}$$

Hence it can be easily shown that

$$k_1^0(R,x,t) = \frac{x(t^2-h^2)}{Rh\sigma}, \tag{A 17c}$$

$$k_1^1(R,x,t) = \frac{t^2-h^2}{Rh\sigma}\left[\frac{x^2}{\sigma}(t^2-h^2)\left(\frac{4}{\sigma}+\frac{1}{h^2}\right)+\frac{4x^2}{\sigma}-1\right], \tag{A 17d}$$

$$k_0^0(R,x,t) = \frac{h}{\sigma}, \tag{A 17e}$$

$$k_0^1(R,x,t) = \frac{x}{\sigma^2}\left[\frac{4h}{\sigma}(t^2-h^2)-(t^2-3h^2)\right], \tag{A 17f}$$

where

$$\sigma = [(t^2-R^2-x^2)^2+4x^2t^2]^{\frac{1}{2}}, \tag{A 18}$$

$$H'(R,x) = \frac{h_1(1-h_1^2)}{R\sigma_1}, \tag{A 19a}$$

$$H''(R,x) = \int_0^1 \frac{t}{\sigma}\left[h-\frac{x^2(t^2-3h^2)}{h\sigma}+\frac{4hx^2(t^2-h^2)}{\sigma^2}\right]dt, \tag{A 19b}$$

with h_1 and σ_1 defined by (A 17*b*) and (A 18) respectively with $t = 1$.

For the purpose of numerical integration of the definite integrals in (2.34) and $H''(R,x)$, the functions k_ν^μ given by (A 17) and the integrand in (A 19*b*) should be determined for small values of t by L'Hospital's rule or from their Taylor approximations.

REFERENCES

Brenner, H. 1961 *Chem. Engng Sci.* **16**, 242.

Dagan, Z. 1980 Entrance effects in Stokes flow through a pore. Ph.D. dissertation, City University of New York.

Dagan, Z., Weinbaum, S. & Pfeffer, R. 1982 *J. Fluid Mech.* **115**, 505–523.

Davis, A. M. J., O'Neill, M. E. & Brenner, H. 1981 *J. Fluid Mech.* **103**, 183.

Erdélyi, A., Magnus, W., Oberhettinger, F. & Tricomi, F. G. 1954 *Tables of Integral Transforms*, vols 1 & 2. McGraw-Hill.

Fahraeus, R. & Lindqvist, T. 1931 *Am. J. Physiol.* **96**, 562.

Ganatos, P., Pfeffer, R. & Weinbaum, S. 1978 *J. Fluid Mech.* **84**, 79.

Ganatos, P., Pfeffer, R. & Weinbaum, S. 1980 *J. Fluid Mech.* **99**, 775.

Ganatos, P., Weinbaum, S. & Pfeffer, R. 1980 *J. Fluid Mech.* **99**, 739.

Gluckman, M. J., Pfeffer, R. & Weinbaum, S. 1971 *J. Fluid Mech.* **50**, 705.

Goldman, A. J., Cox, R. G. & Brenner, H. 1967*a* *Chem. Engng Sci.* **22**, 637.

Goldman, A. J., Cox, R. G. & Brenner, H. 1967*b* *Chem. Engng Sci.* **22**, 653.

Haberman, W. L. & Sayre, R. M. 1958 *David W. Taylor Model Basin Rep.* no. **1143**, Washington, D.C.

Happel, J. & Brenner, H. 1973 *Low Reynolds Number Hydrodynamics*, 2nd ed. Noordhoff.

Leichtberg, S., Pfeffer, R. & Weinbaum, S. 1976 *Int. J. Multiphase Flow* **3**, 147.

Leichtberg, S., Weinbaum, S., Pfeffer, R. & Gluckman, M. J. 1976 *Phil. Trans. R. Soc. Lond.* A **282**, 585.

Sampson, R. A. 1891 *Phil. Trans. R. Soc. Lond.* A **182**, 449.

Tranter, C. J. 1951 *Quart. J. Math.* **2**, 60.